

## X-Ray Compton-Raman Scattering from Atomic Inner-Shell Electrons

Kazumichi Namikawa and Sukeaki Hosoya

*The Institute for Solid State Physics, The University of Tokyo, Roppongi, Minato-ku, Tokyo 106, Japan*

(Received 21 February 1984)

Inelastic scattering of  $^{241}\text{Am}$  59.57-keV  $\gamma$  rays from Cu and Fe was measured in coincidence with the  $K$ -fluorescence x rays. The spectrum due to the scattering by the  $K$ -shell electrons shows the coexistence of a Compton-type and a Raman-type scattering. Double-photon Thomson-type scattering is also identified, which is weaker than the usual Compton scattering by a factor of about  $4 \times 10^{-3}$ .

PACS numbers: 78.70.Ck

X-ray inelastic scattering by a free electron is completely characterized by the energy and the momentum conservation laws. This phenomenon is the well-known Compton scattering. In contrast to Compton scattering, the feature of x-ray inelastic scattering by a bound electron varies with the value of  $ka$  even when  $\hbar\omega_1 \gg E_b$ ,<sup>1,2</sup> where  $\hbar k$  is the momentum transfer and  $a$  is the radius of the binding orbital, while  $\hbar\omega_1$  and  $E_b$  are the energies of the incident photon and the binding orbital, respectively.

When  $ka \gg 1$ , the peak position of the spectrum is determined only by the primary energy and by the scattering angle, but it is independent of the type of scattering atom. This is a distinct feature of Compton scattering, although Doppler broadening of the normal Compton line takes place: The spectrum includes information on the momentum distribution of the electrons in the initial state. This phenomenon is Compton scattering by a bound electron. On the contrary, when  $ka < 1$ , the peak position of the spectrum corresponds to the absorption edge of the relevant atomic orbital, but it depends neither on the scattering angle nor on the primary photon energy. The spectrum, in this case, is related to the dipole moment strength per energy. This phenomenon is x-ray Raman scattering. When  $ka \geq 1$ , so-called Compton-Raman scattering takes place. In this case, transition phenomena between the above two typical cases, Compton and Raman type, are expected to appear. The nature of the phenomena is not yet well understood, partly because there has been no reliable low-energy experiment so far which investigated separately the spectrum due to electrons in a single shell.

In the present experiment, inelastic scattering spectra from  $K$ -shell electrons have been measured on Cu ( $ka = 1.02$ ) and Fe ( $ka = 1.16$ ) by means of coincidence counting between the low-energy  $\gamma$  rays scattered and the  $K$ -fluorescence x rays subsequently emitted.<sup>3-9</sup> By this technique, certain basic properties have been revealed for the x-ray inelastic

scattering in the region where  $ka \geq 1$ .

The experimental apparatus, arranged as shown in Fig. 1, consisted of a  $\gamma$ -ray source, a collimator, a sample, a  $\gamma$ -ray detector, and an x-ray detector. The  $\gamma$ -ray source was 100 mCi  $^{241}\text{Am}$  placed at the bottom of the collimator in a lead block. The  $\gamma$ -ray beam was collimated to about  $\pm 10^\circ$  through the beam pass. The primary energy of the photon utilized was 59.57 keV. The samples investigated were a 50- $\mu\text{m}$ -thick copper foil and a 100- $\mu\text{m}$ -thick iron foil. Each foil, 60 mm  $\times$  60 mm in area, was held in a 6-cm  $\times$  6-cm slide mount. Both the  $\gamma$ -ray detector and the x-ray detector were pure Ge solid-state detectors. The effective area of the former was 100 mm<sup>2</sup> in size, 5 mm thick, and that of the latter was 300 mm<sup>2</sup> in size, 10 mm thick. The resolution of the former was 560 eV at 59.57 keV and that of the latter was 550 eV at 6.39 keV, while the detection efficiencies were practically constant in the relevant energy region for both detectors.

Coincidence counting was carried out by the use of a pair of timing single-channel analyzers, a fast coincidence circuit, a linear gate, and a multichannel analyzer. The resolving time of the coincidence was set at 60 nsec. The counting rate of the inelas-

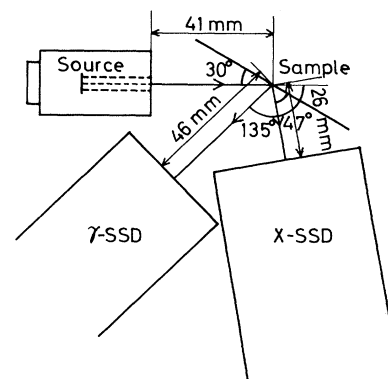


FIG. 1. The experimental arrangement for the separate measurement of the inelastically scattered  $\gamma$ -ray spectrum due to  $K$ -shell electrons.

tically scattered  $\gamma$  ray was 74.8 counts/sec for Cu and 123 counts/sec for Fe, while that of the fluorescence x ray was 421 counts/sec for Cu and 184 counts/sec for Fe. A measurement of the raw coincidence spectrum, including the chance and the false coincidences, was carried out for  $5 \times 10^5$  sec. Then a measurement of the chance coincidences was carried out also for the same amount of time, but out of coincidence by 200 nsec. Five pairs of such data were accumulated. The effective coincidence spectrum was obtained as a difference between the sum of the five runs of the raw coincidence spectra and the sum of the chance-coincidence spectra. The mean counting rate for the chance coincidences was  $1.96 \times 10^{-3}$  count/sec for Cu and  $1.36 \times 10^{-3}$  count/sec for Fe. These values agreed within 1% or so with the values estimated statistically. The counting rate of the effective coincidence was found to be  $1.76 \times 10^{-3}$  count/sec for Cu and  $1.60 \times 10^{-3}$  count/sec for Fe.

The effective coincidence spectra obtained for Cu and for Fe are shown in Figs. 2(a) and 2(b), respectively, where the counts in five channels were added and a correction for the absorption has been made. For comparison, the spectrum obtained without coincidence is illustrated in Fig. 2(c). The solid lines in Figs. 2(a) and 2(b) are obtained by least-squares fittings of each spectrum. The arrows indicated by  $E_0$  and  $E_b$  show the primary energy of the incident photons and  $E_0$  minus the binding edge of the  $K$ -shell electrons, respectively. The coincidence spectra, Figs. 2(a) and 2(b), consist of four peaks C, C', R, and DT, while spectrum 2(c) consists of the well-known Compton peak C and the coherent scattering peak T.

The characteristic features of the spectra in Figs. 2(a) and 2(b), except for the peak C', are scarcely affected by false coincidences such those as due to (1) multiple scattering, or (2)  $K$ -shell excitation by the recoiled outer-shell electrons. The probability of (1) is negligible because the ratio of double scattering to single scattering in the present case is estimated to be about the order of 1%; that of (2) is small enough practically because the distinct high-energy tail of the normal Compton spectrum, which is evidence for the contribution from the outer-shell electrons, can hardly be found in spectra 2(a) and 2(b). On the contrary, the peak C' is attributed to the false coincidences due to sequential Compton scattering: first at the sample and then at the x-ray detector,<sup>7</sup> where the x-ray detector measured the energy of the recoil electron remaining in the detector and the  $\gamma$ -ray detector measured the photon energy after two scatterings.

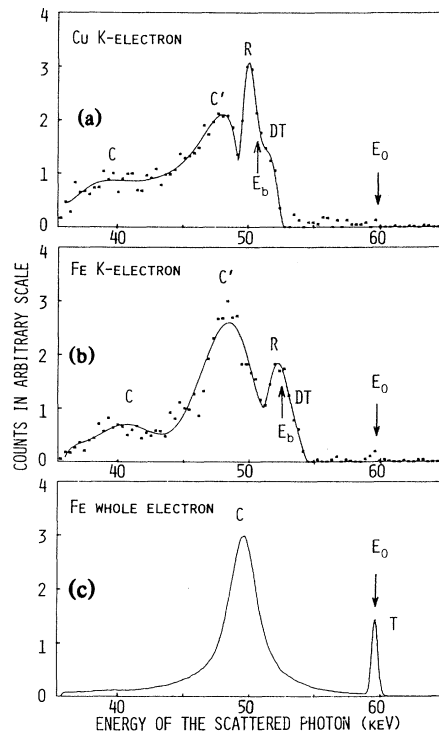


FIG. 2. The  $\gamma$ -ray inelastic scattering spectra, (a), (b) due to the  $K$ -shell electrons, and (c) due to all shells. The peaks C, R, and DT in (a) and (b) are due to Compton-type, Raman-type, and double-photon Thomson-type scattering, respectively, while the peak C' is due to false coincidences. The peaks C and T in (c) are due to Compton scattering and the coherent scattering, respectively. The maximum in (a) and (b) corresponds to 231 counts and 216 counts, respectively. The solid lines in (a) and (b) are least-mean-squares fittings.

The low-energy region of the spectra in Fig. 2(a) and 2(b) corresponds to scattering with a large energy transfer, and thus the kinetic energy of the recoil electron is high; the wave function of the electron is expected to behave as a plane wave. In such cases, the transition probability of the scattering becomes large when  $\vec{p} \sim \vec{p}_0 + \hbar \vec{k}$ , where  $\vec{p}_0$  and  $\vec{p}$  are the initial and the final momentum of the recoil electron, respectively. Consequently, Compton-type scattering takes place. However, the energy transferred is not  $(\vec{p}_0 + \hbar \vec{k})^2/2m$ , but rather  $(\vec{p}_0 + \hbar \vec{k})^2/2m + E_b$ .<sup>10</sup> Both regions C in Figs. 2(a) and 2(b) are characterized by large widths and by peaks appearing at 39.0 keV for Cu and 40.7 keV for Fe. These values are subject to the conservation of energy mentioned above, though they are a little lower than the values relevant to each case for  $\vec{p}_0 = 0$ : 42.1 keV for Cu and 43.6 keV for Fe. These shifts in peak energy are reasonable because

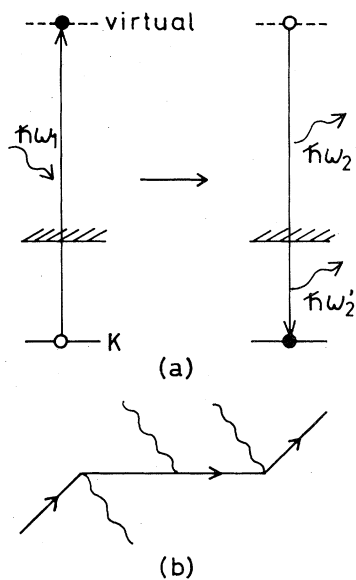


FIG. 3. (a) Transition mechanism corresponding to the double-photon Thomson scattering. (b) One of the third-order diagrams relevant to the above process.

the Compton spectrum due to inner-shell electrons by no means corresponds to the usual Compton profile—an integral of the momentum density over the equi- $p_0^2$  plane, where  $p_0^2$  is the projection of the electron momentum along the direction of  $\vec{k}$ . Therefore, the peaks C in Figs. 2(a) and 2(b) are assigned to Compton scattering due to K-shell electrons. On the other hand, the spectral regions near the binding edge in 2(a) and 2(b) correspond to a process with small energy transfer. The wave function of the relevant electron is an eigenfunction of the crystal orthogonal to the inner-shell orbitals. In this case, Raman-type scattering is the predominant scattering process. The Raman-type scattering is known to give a profile similar to that of absorption on the lower-energy side of the binding edge.<sup>1,2,11</sup> Characteristic features of the peaks R in in Figs. 2(a) and 2(b) are those of Raman scattering mentioned above.

One of the most remarkable features of the spectra in Figs. 2(a) and 2(b) is the coexistence of the Compton-type peak C and the Raman-type peak R. It is worthwhile to note the change in the relative intensity of these peaks between 2(a) and 2(b): The ratio of the intensities,  $I_R/I_C$ , changes from 0.83 for Cu to 0.62 for Fe. This change suggests that the switchover between these two scattering processes takes place, according to the variation of the value  $ka$ , not by the removal of a single peak but by the growth of one peak and the decrease of the other.

The bandlike spectral features DT in Figs. 2(a) and 2(b) appear in the energy region where the energy transfer is smaller than the excitation energy of the K-shell electrons. Inelastic scattering accompanied by such excitation is not allowed in a second-order process, because all the levels in this region have been occupied. Those spectra, however, probably exist if a third-order process as illustrated in Fig. 3(a) is taken into consideration, where  $\hbar\omega_1 = \hbar\omega_2 + \hbar\omega_2'$  is fulfilled. One of the graphs relevant to the process in Fig. 3(a) is shown in Fig. 3(b). In the present measurement, such spectra corresponding to the process in Fig. 3 may become bandlike because the x-ray single-channel analyzer has been set to select only those photons whose energy  $\hbar\omega_2'$  is in the region, including K-series fluorescence x-ray spectra, from 6.9 to 9.7 keV for Cu and from 5.4 to 7.7 keV for Fe. The cutoffs of the spectra in Figs. 2(a) and 2(b) obviously correspond to the lower limits of these values. The cross section relevant to the peaks DT amounts to about  $4 \times 10^{-3}$  of that of the ordinary Compton scattering in Fig. 2(c) when the solid angle of the detector, the bandwidth of the spectra, and the effects of absorption are taken into consideration. This small cross section strongly suggests that the peaks DT are due to the third-order scattering process.<sup>12</sup> In conclusion, the peaks DT can be assigned to a part of the double-photon Thomson scattering.<sup>13</sup>

<sup>1</sup>Y. Mizuno and Y. Ohmura, J. Phys. Soc. Jpn. **22**, 445 (1967).

<sup>2</sup>M. Kuriyama, Acta Crystallogr. **A27**, 643 (1971).

<sup>3</sup>D. Brini, E. Fuschini, N. T. Grimellini, and D. S. R. Murty, Nuovo Cimento **16**, 727 (1960).

<sup>4</sup>Z. Sujikowski and B. Nagel, Ark. Fys. **20**, 323 (1961).

<sup>5</sup>J. W. Motz and G. Missoni, Phys. Rev. **124**, 1458 (1961).

<sup>6</sup>J. Varma and M. A. Eswaran, Phys. Rev. **127**, 1197 (1962).

<sup>7</sup>S. Shimizu, Y. Nakayama, and T. Mukoyama, Phys. Rev. **140**, A806 (1965).

<sup>8</sup>T. Fukamachi and S. Hosoya, Phys. Lett. **38A**, 341 (1972).

<sup>9</sup>M. Pradoux, H. Meunier, J. Bauman, and G. Roche, Nucl. Instrum. Methods **112**, 443 (1973).

<sup>10</sup>P. Eisenberger and P. M. Platzman, Phys. Rev. A **2**, 415 (1970).

<sup>11</sup>T. Suzuki, J. Phys. Soc. Jpn. **22**, 1139 (1967).

<sup>12</sup>W. Heitler, *The Quantum Theory of Radiation* (Oxford Univ. Press, Oxford, England, 1953), 3rd ed., pp. 224–229.

<sup>13</sup>I. Freund and B. F. Levine, Phys. Rev. Lett. **23**, 854 (1969).